The 8th European Congress on Computational Methods in Applied Sciences and Engineering
ECCOMAS Congress 2022
5-–9 June 2022, Oslo, Norway

EFFECT OF LASER BEAM SCATTERING IN SPH-SIMULATION OF DEEP PENETRATION LASER BEAM WELDING

Daniel Sollich[1], Florian Fetzer[2] and Peter Eberhard[1]

[1] Institute of Engineering and Computational Mechanics
University of Stuttgart
Pfaffenwaldring 9, 70569 Stuttgart, Germany
{daniel.sollich, peter.eberhard}@itm.uni-stuttgart.de, www.itm.uni-stuttgart.de/en

[2] Institut für Strahlwerkzeuge
University of Stuttgart
Pfaffenwaldring 43, 70569 Stuttgart, Germany
f_fetzer@outlook.de, www.ifsw.uni-stuttgart.de/en

Key words: Laser Beam Welding, SPH, Ray Tracing Laser Beam, Laser Beam Scattering, Melt Dynamics, Capillary Stability

Abstract. The effect of laser beam scattering on capillary stability and melt dynamics is investigated simulatively for deep penetration laser beam welding. The mesh-free Lagrangian Smoothed Particle Hydrodynamics (SPH) method is coupled with a ray-tracing scheme. The SPH model covers fluid and thermodynamics, including temperature-dependent surface tension, recoil pressure, heat conduction, and phase transitions. The ray tracer models the laser-material interaction by tracking the propagation of light rays within the capillary according to the laws of geometrical optics, and taking into account multiple reflections and scattering. Surface scattering due to surface roughness, and volume scattering due to condensed droplets or local changes of the complex refractive index in the vapor plume are evaluated separately. For surface scattering, the reflections at the material surface are divided into a specular part and a diffuse part with randomly reflected rays. For volume scattering, the Henyey-Greenstein model is used to specify the angular distribution of the scattered light ray. The effect of scattering is examined for laser beam welding of aluminum and titanium. The results show that volume scattering has a stabilizing effect on the capillary for the highly reflective material aluminum, while the effect of surface scattering is small for both materials.

1 INTRODUCTION

Deep penetration laser beam welding is a joining technique widely used for its deep weld seams, high efficiency, and ease of automation. In the process, a vapor-filled capillary is formed by the high intensities on the irradiated surface and subsequent evaporation of the material. The laser beam is reflected multiple times within the capillary resulting in a complex distribution of the absorbed laser power. Scattering of the laser beam may affect the locally absorbed laser power and thus the capillary shape and melt dynamics. Little is known so far about the influence of scattering on the process and the formation of instabilities such as pores, spatter, or humping.

In addition to experimental observations, numerical simulations provide further insight into the process. Advanced simulation models include important physical effects such as heat transfer by heat conduction, phase transitions, temperature-dependent surface tension, and evaporation-induced recoil pressure. An overview of laser welding simulations using mesh-based methods such as the Finite Element Method (FEM) or the Finite Volume Method (FVM) is given in [1]. Mesh-free particle methods such as the Smoothed Particle Hydrodynamics (SPH) method have received more attention in recent years due to their advantageous formulation of free surfaces and multiphase flows with phase transitions. To date, the SPH method is able to successfully capture the main characteristics of deep penetration laser beam welding in [2], laser beam drilling in [3], and Selective Laser Melting (SLM) in [4, 5, 6].

In the modeling of scattering, a distinction must be made between surface and volume scattering. Surface scattering occurs at the capillary surface due to the fine surface structures. In the process simulations, surface roughness is often neglected during ray tracing, and specular reflections from an ideally smooth surface are assumed as in [2, 3]. Volume scattering is caused by inhomogenities within the capillary, such as condensed droplets or local changes in the complex refractive index in the vapor plume. Volume scattering can be modeled by applying the Henyey-Greenstein model [7] or the Mie Theory [8]. Both models are used to define a phase function that describes the angular distribution of the light intensity scattered by a particle at a given wavelength. While the Mie theory requires the solution of Maxwell's equation, the Henyey-Greenstein model is a simple model that approximates the phase function using a single parameter. Scattering is addressed in the deep penetration laser beam welding simulation in [9], where only the effect of volume scattering is considered by the Henyey-Greenstein model.

In this work, the effects of surface and volume scattering on the capillary and melt dynamics are evaluated separately by coupling the SPH method with a ray-tracing scheme. The SPH model and the ray tracer are briefly introduced in Section 2. Surface and volume scattering are modeled as described in Section 3. For surface scattering, a diffuse reflection mechanism is superimposed to the specular reflections, and for volume scattering, the Henyey-Greenstein model is applied. In Section 4, the influence of scattering is examined, first on the distribution of the absorbed laser power and then on the capillary geometry and the melt dynamics.

2 MODELING APPROACH

The simulation model for deep penetration laser beam welding can be divided into two parts. The first part, the SPH model in Section 2.1, covers the discretization of the continuum including fluid and thermodynamics. The second part, the laser-material interaction in Section 2.2, includes the calculation of the energy input of the laser beam using a ray-tracing scheme. The modeling approach is only briefly presented below. Please refer to [2] for a detailed description of the simulation model.

2.1 SPH Model

The SPH method is a mesh-free, Lagrangian particle method that represents a continuum by a set of freely moving particles. The properties of the particles are determined by a weighted interpolation from their neighboring particles using the smoothing kernel function. In the SPH model, the weakly-compressible formulation of Monaghan [10] is applied. The governing equa-

tions guaranteeing the conservation of mass, momentum and energy are given by

$$\frac{\mathrm{d}\rho}{\mathrm{d}t} = -\rho\nabla\cdot\boldsymbol{v}\,, \tag{1}$$

$$\frac{\mathrm{d}\boldsymbol{v}}{\mathrm{d}t} = -\frac{1}{\rho}\nabla p + \frac{\mu}{\rho}\nabla^2\boldsymbol{v} + \boldsymbol{a}_g + \boldsymbol{a}_s + \boldsymbol{a}_r\,, \tag{2}$$

$$\rho\frac{\mathrm{d}e}{\mathrm{d}t} = \lambda\nabla^2 T + \dot{q}_V + \dot{q}_r\,, \tag{3}$$

where ρ is the density, t the time, $\boldsymbol{v}$ the velocity, p the pressure, μ the dynamic viscosity, $\boldsymbol{a}_g$, $\boldsymbol{a}_s$, and $\boldsymbol{a}_r$ the accelerations due to gravitational, surface tension, and recoil pressure force, e the internal energy, λ the heat conductivity, $\dot{q}_\mathrm{V}$ a volumetric source term to account for the energy input of the laser beam, and $\dot{q}_\mathrm{r}$ the heat losses from the evaporating material.

The surface tension force including the Marangoni force is calculated for the liquid melt based on the continuum surface force model. For the solid phase, elastic material behavior is assumed. Heat transfer in the material is modeled by heat conduction. The thermally induced volume expansion and contraction of the material is considered by a temperature-dependent formulation for the density. In addition to the density, the thermal conductivity, heat capacity, and dynamic viscosity are modeled as temperature-dependent material parameters. Phase transitions are treated based on the enthalpy method and include the latent heat of fusion and evaporation. The phase transitions considered are melting, solidification, and evaporation. During evaporation, the recoil momentum of the expanding vapor acting on the liquid phase is taken into account by the recoil pressure. After a particle is completely evaporated, it is removed from the simulation. Consequently, the flow of the vapor phase and condensation are not considered.

2.2 Laser-Material Interaction

In deep penetration laser beam welding, the laser beam is reflected multiples times at the capillary surface, resulting in a complex spatial distribution of the absorbed laser power. To estimate the locally absorbed laser power, the ray-tracing scheme proposed in [11] is applied. The laser beam is represented by numerous rays that are randomly generated depending on the given intensity profile of the laser beam. The propagation of each ray is traced, where at each reflection the locally absorbed laser power is calculated using the Fresnel equations [12]. For each ray, multiple reflections are considered until no relevant interaction between the ray and the capillary surface is detected anymore or a maximum number of reflections is reached.

The SPH model in Section 2.1 is coupled with the ray tracer to perform a transient simulation of the laser welding process. In the SPH simulation, the ray tracer is called at a user-defined time interval starting a co-simulation loop. As input, the ray tracer requires a triangular surface mesh of the capillary. The mesh is generated by first detecting surface particles in the SPH simulation and then performing a surface reconstruction by the Ball-Pivoting Algorithm [13]. The ray tracer determines the locally absorbed irradiance on the surface mesh, which is afterwards transformed in the SPH simulation into the numerous heat source particles positioned in the center of each triangle. The SPH simulation is continued with these dynamically added heat source particles until the next co-simulation loop is started. The data between the SPH simulation and the ray tracer is exchanged via a TCP/IP network connection.

3 SCATTERING ALGORITHMS

The transient behavior of the capillary strongly depends on the absorbed laser power and its spatial distribution on the material surface. As schematically shown in Fig. 1, scattering of the laser beam can effect the distribution of the locally absorbed laser power. On the one hand by surface scattering due to fine surface structures, and on the other hand by volume scattering due to condensed droplets or local changes of the complex refractive index in the vapor plume. The modeling of surface and volume scattering is described in more detail below. Both models are implemented in the ray tracer described in Section 2.2.

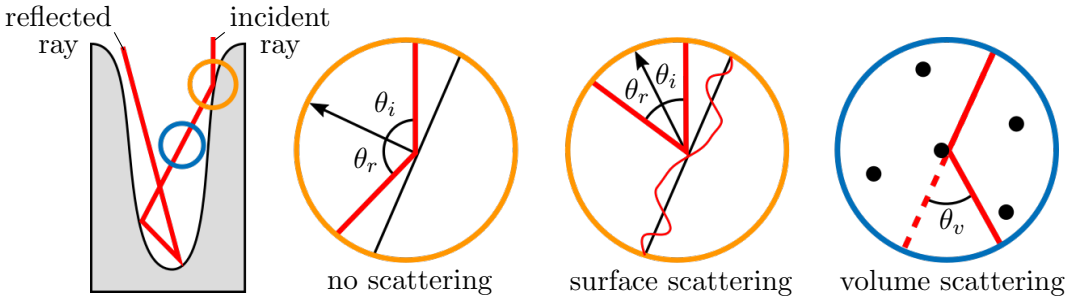

Figure 1: Schematic illustration of surface and volume scattering within the capillary during deep penetration laser beam welding.

3.1 Surface Scattering

Without surface scattering, only specular reflections of the rays on an ideally smooth surface are assumed. To account for surface scattering, a diffuse reflection mechanism can be superimposed to the specular reflections. For the modeling of the diffuse reflections, the reflected ray is randomly chosen in any spatial direction. The only requirement is that the ray must not penetrate through the triangles. The angle of incidence is equal to the angle of reflection $\theta_i = \theta_r$ for specular and diffuse reflections as shown in Fig. 1. The fraction of specular and diffuse reflections can be specified by $n_{\text{diff}} = [0, 1]$, where $n_{\text{diff}} = 0$ allows only specular reflections without surface scattering, and $n_{\text{diff}} = 1$ only diffuse reflections at the material surface.

3.2 Volume Scattering

In contrast to surface scattering, where the ray is reflected at the capillary surface, for volume scattering the deflection of the ray takes place within the capillary. To model volume scattering, the distance of the ray to a scattering event, and the direction of the scattered ray must be determined. The scattering direction $\boldsymbol{r}_v$ is obtained from the scattering angle θ_v and a randomly chosen normalized vector $\boldsymbol{n}$ perpendicular to the normalized direction of the incident laser beam $\boldsymbol{r}_{\text{laser}}$ by

$$\boldsymbol{r}_v = \frac{\boldsymbol{r}_{\text{laser}} + \boldsymbol{n} \tan \theta_v}{\|\boldsymbol{r}_{\text{laser}} + \boldsymbol{n} \tan \theta_v\|} \,. \tag{4}$$

To calculate the scattering angle θ_v of the ray, the Henyey-Greenstein model in [7] is used.

In this model, the angular distribution of the scattered ray is defined by the phase function

$$p(\theta_v) = \frac{1 - g^2}{4\pi \left(1 + g^2 - 2g\cos\theta_v\right)^{\frac{3}{2}}}, \tag{5}$$

where $g = [-1, 1]$ is the anisotropy factor. In Fig. 2 the phase function is plotted as a function of the anisotropy factor. For $g = 0$, the phase function does not depend on the scattering angle resulting in isotropic scattering. In contrast, forward scattering dominates for $g > 0$ and backward scattering for $g < 0$. The scattering angle can be determined, as shown in Fig. 2, using the inverse of the normalized integral of the phase function at a randomly chosen value between 0 and 1.

The calculation of the distance d to a scattering event is given by

$$\mu_v = 1 - \exp\left(-\lambda_v d\right), \tag{6}$$

where $\mu_v = [0, 1]$ is the probability per unit length that a ray is deflected from its previous direction, and λ_v a coefficient to control the strength of the scattering. By specifying λ_v and a randomly chosen value for μ_v, the distance to a scattering event can be determined. The scattering event is ignored, if the event occurs outside the capillary, i.e. above the workpiece, or at a distance larger than the triangle to be hit. After a scattering event, a new triangle is searched in direction of the deflected ray to calculate the next reflection on the capillary surface.

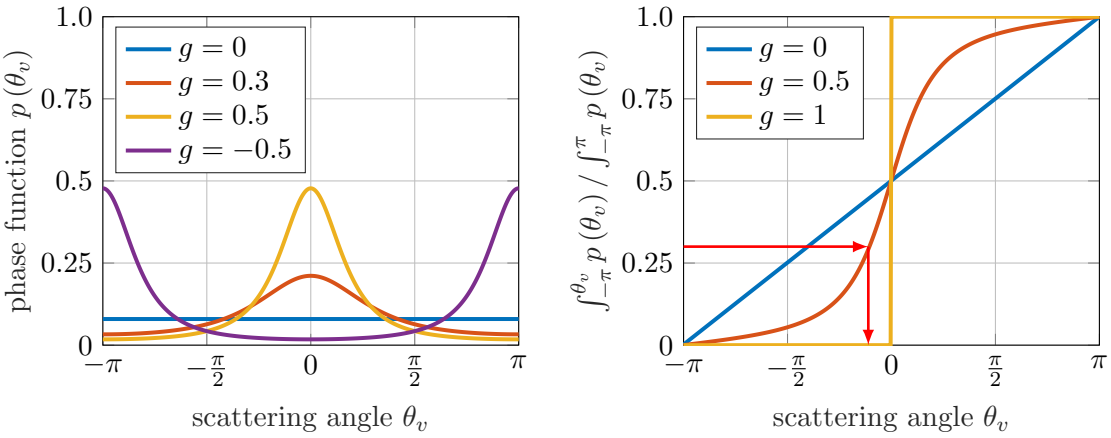

Figure 2: Determination of the scattering angle using the Henyey-Greenstein model in [7].

4 SIMULATION RESULTS

The simulation results are structured into two parts. First, the effect of scattering on the absorbed laser power is analyzed in Section 4.1 using a fixed capillary geometry. Next, the effect of scattering on the transient behavior of the capillary and the melt flow are examined in Section 4.2 for the full process simulation. In the following, surface and volume scattering are evaluated separately and compared to the reference simulation without scattering. A combination of both scattering types is not examined.

4.1 Effect of Scattering on the Local Absorption Behavior in the Capillary

In the following example, the influence of scattering on the distribution of the absorbed laser power within the capillary is examined. The absorption behavior is analyzed here first decoupled from the process simulation by using a fixed capillary geometry. The geometry is reconstructed using the gray levels of the images in [14] with the experimental setup given in [15]. The laser beam has a power of 1 kW, a Gaussian intensity distribution, and a focal diameter of 0.1 mm. The position of the laser beam relative to the capillary front is set to half the focal diameter.

Figure 3 shows the locally absorbed irradiance in dependence on the scattering type for the highly reflective aluminum and the highly absorbing titanium. The results of the reference without scattering (N) and with only surface scattering (S) are very similar. In both cases, most of the power is absorbed at the capillary tip. For only volume scattering (V), the absorbed power is better distributed in the capillary, resulting in a much lower absorbed power at the capillary tip. The total absorbed power decreases for both surface and volume scattering. The exact value depends strongly on the scattering parameters for only volume scattering, and is significantly lower for the chosen parameters $\lambda = 3.5\,\mathrm{mm}^{-1}$ and $g = 0$. In the case of titanium, more energy is absorbed at the first reflections due to the high absorptivity of the material. The effect of scattering is similar to that of aluminum.

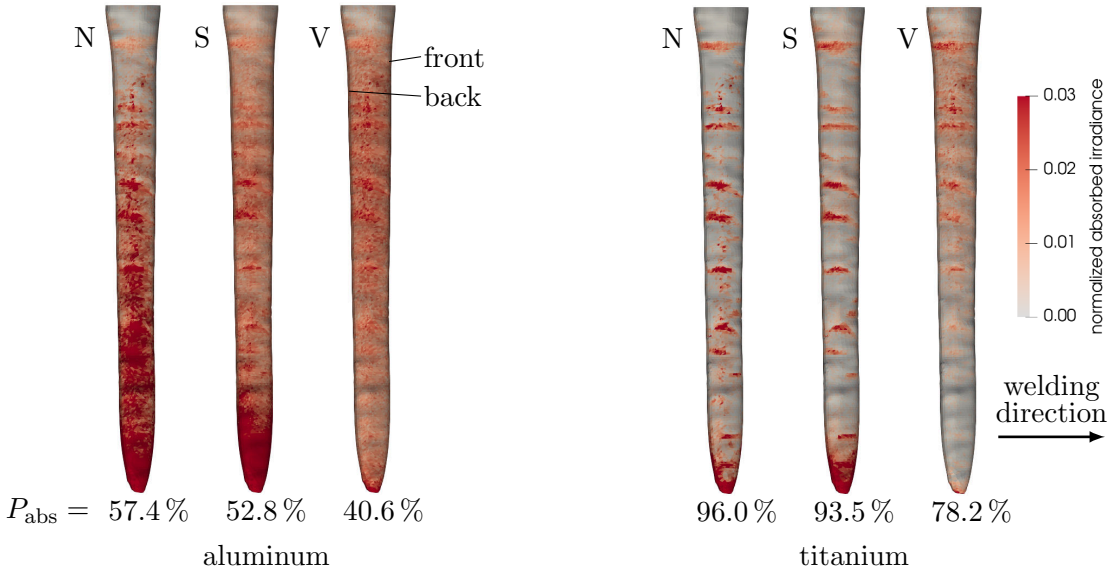

Figure 3: Distribution of absorbed irradiance and total absorbed laser power P_{abs} in the cross section of the reconstructed capillary of the experiments in [14] without scattering (N), with only surface scattering $n_{\mathrm{diff}} = 1$ (S), and with only volume scattering of $\lambda = 3.5\,\mathrm{mm}^{-1}$ and $g = 0$ (V) for aluminum and titanium.

4.2 Effect of Scattering in the Deep Penetration Laser Beam Welding Simulation

In the following examples, deep penetration laser beam welding is simulated for aluminum and titanium, now including the full process. The aim is to examine the influence of surface and volume scattering on the transient behavior of the capillary and the fluid dynamics of the melt.

For aluminum, the process parameters are chosen according to [14], with the validation of the simulation model given in [2]. The laser beam with Gaussian intensity distribution, a power of 1 kW, and a focal diameter of 0.1 mm, is focused on the top surface of the workpiece, and is moved along the x-axis at a constant feed rate of 0.1 m/s. During ray tracing, 100,000 rays are used to represent the laser beam. The particle setup of the simulated workpiece is shown in Fig. 4. The workpiece has dimensions $2.08 \times 1.60 \times 1.44\,\mathrm{mm}^3$, an adiabatic thermal boundary, and an initial temperature of 293 K. Multilevel particle refinement with three refinement levels is applied according to [16] to keep the number of solid particles low, while maintaining the macroscopic thermal properties of the workpiece. The particle spacing for the finest resolution level is 0.02 mm.

For the reference simulation without scattering, the transient behavior and standard deviation of the capillary depth and absorbed power of the laser beam are shown in Fig. 5. Strongly correlated fluctuations in capillary depth and absorbed power are observed. When the capillary depth is low, the absorbed power decreases and vice versa. The reason for the correlation is that the laser beam is reflected more often with increasing capillary depth and thus transfers more power to the material surface.

A typical fluctuation of the capillary depth including the melt flow is shown in Fig. 6. Most of the laser power is absorbed at the capillary tip causing local vaporization there. The resulting recoil pressure accelerates the melt upward along the back wall. Melt bridges form in the upper part of the capillary, dividing it and preventing the laser beam from being reflected to the lower part. The absorbed power drops abruptly until the previous capillary depth is reached again.

The influence of surface and volume scattering is shown separately in Fig. 7 using the mean and standard deviation of the capillary depth. For only surface scattering, there is no significant effect on the mean depth and the standard deviation. Only the mean depth is slightly increased for a diffuse reflection fraction of $n_{\mathrm{diff}} = 0.2$ and $n_{\mathrm{diff}} = 0.5$. The minor effect can be explained by the similar absorption behavior shown in Fig. 3, where large absorbed power is observed at the capillary tip for the simulations without scattering and with only surface scattering. In

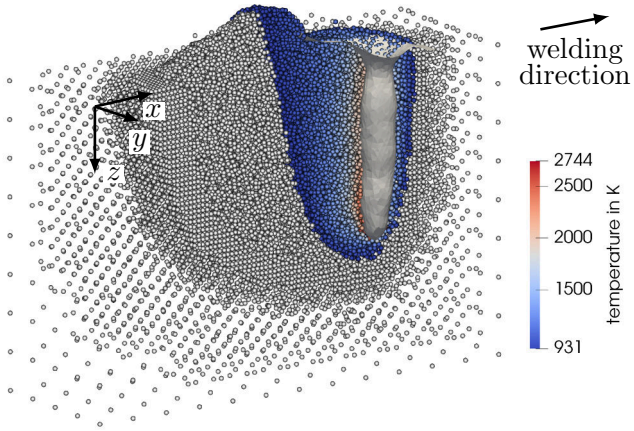

Figure 4: Capillary geometry and temperature distribution in the cross section of the melt pool during deep penetration laser beam welding of aluminum at $t = 8\,\mathrm{ms}$. The temperature is shown only for the melt to be distinguished from the solid workpiece.

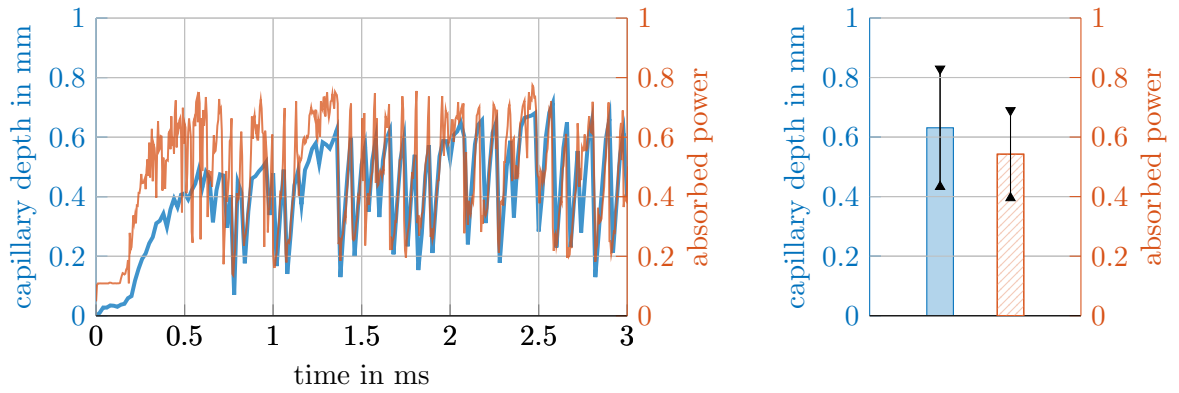

(a) transient behavior

(b) standard deviation after 5 ms

Figure 5: Capillary depth and absorbed laser power during deep penetration laser beam welding of aluminum without laser beam scattering.

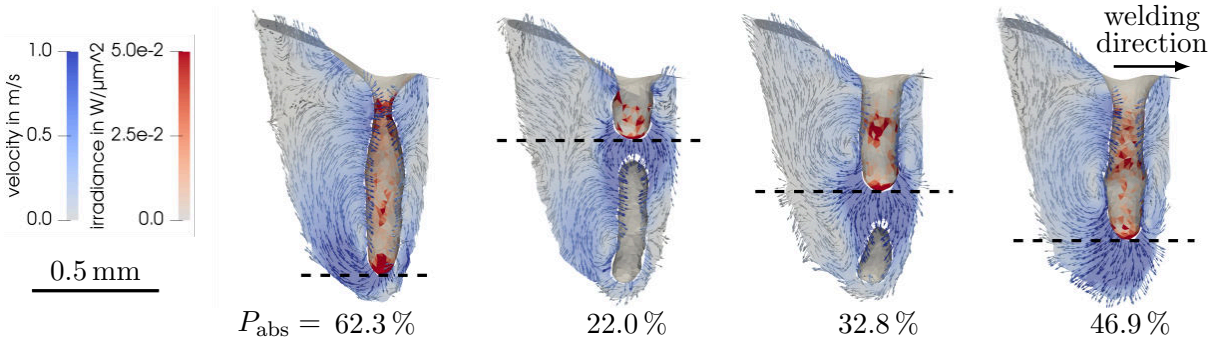

Figure 6: Cross section of the aluminum melt pool showing the collapse of the capillary by the separation of a cavity for $t = 7.32\,\text{ms}$ to $t = 7.38\,\text{ms}$, and without laser beam scattering. The percent values indicate the total absorbed laser power P_{abs} and the dashed black lines the current capillary depth.

the case of only volume scattering, the mean depth remains approximately constant, while a significant decrease in the standard deviation can be seen when varying both the frequency of a scattering event and the distribution of the scattering direction. This effect can be explained by the better distribution of the locally absorbed power in the capillary and the resulting lower absorbed power at the capillary tip.

The flow behavior with only volume scattering is shown in Fig. 8. Due to the lower absorbed power at the capillary tip, the recoil pressure is lower there as in the reference simulation without scattering. Strong acceleration of the melt is no longer noticeable, so that no melt bridges are formed and the shape of the capillary remains approximately constant over time. For aluminum and the given process parameters, volume scattering can thus significantly increase the stability of the capillary in the simulation.

For deep penetration laser beam welding of titanium, the process parameters are chosen

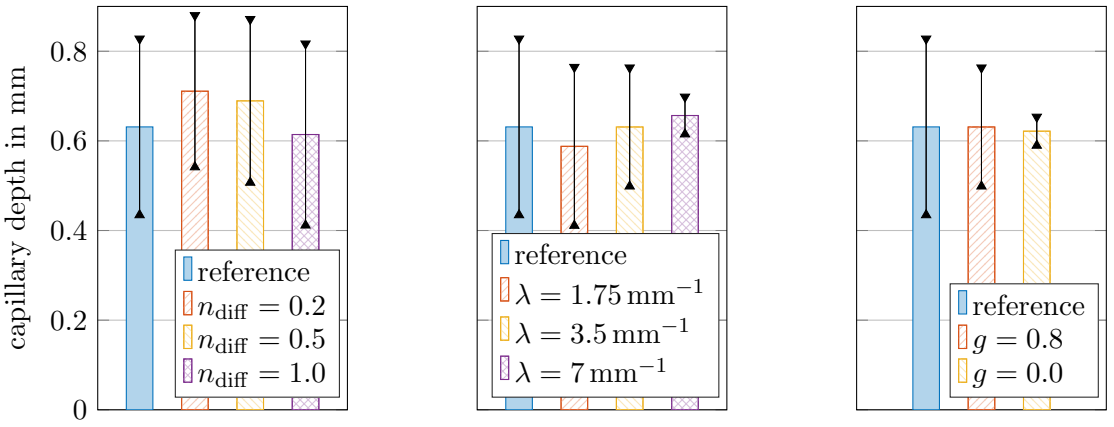

(a) only surface scattering

(b) only volume scattering, $g = 0.8$

(c) only volume scattering, $\lambda = 3.5\,\text{mm}^{-1}$

Figure 7: Mean value and standard deviation (error bars) of the capillary depth in the quasi-steady state after 5 ms for deep penetration laser beam welding of aluminum.

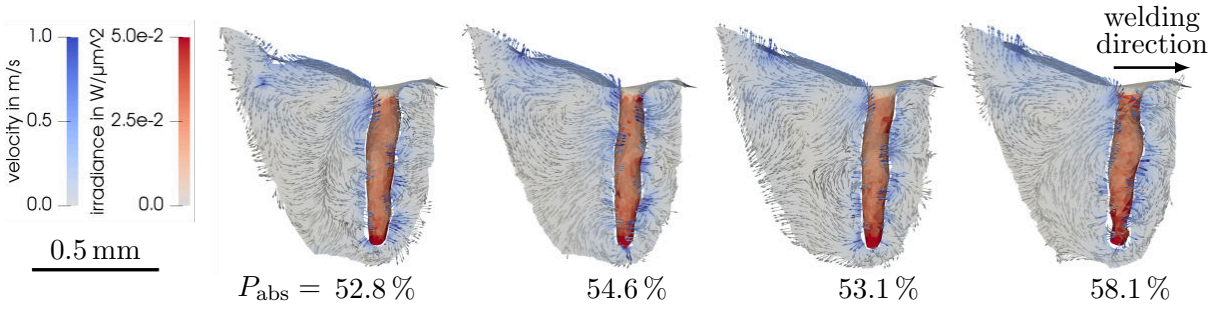

Figure 8: Cross section of the aluminum melt pool with only volume scattering of $\lambda = 3.5\,\text{mm}^{-1}$ and $g = 0$ for $t = 7.32\,\text{ms}$ to $t = 7.38\,\text{ms}$. The percent values indicate the total absorbed laser power P_{abs}.

according to [17]. The laser beam has a power of 84 W, and a focus diameter of 0.1 mm, and is moved along the x-axis with a constant feed rate of 0.15 m/s. The dimensions of the simulated workpiece are $1.47 \times 0.4 \times 0.4\,\text{mm}^3$ with the particle setup shown in Fig. 9. The particle spacing for the finest resolution level is 0.0083 mm. Compared to the simulation with aluminum, the capillary depth and the angle of incline of the capillary front is smaller. The influence of scattering is shown in Fig. 10 using the mean and standard deviation of the capillary depth. For both scattering types, the mean depth decreases, while the standard deviation is approximately constant, because the capillary stability for titanium is already high in the reference simulation without scattering. During ray tracing, the first reflection of the rays occurs mainly at the capillary front and not at its tip as in the aluminum simulation. For surface scattering, the rays are then no longer reflected to the capillary tip as it is the case for specular reflections without scattering. Less energy is absorbed at the tip and the capillary depth decreases. This is also the case for volume scattering, where fewer rays reach the capillary tip due to the scattering events.

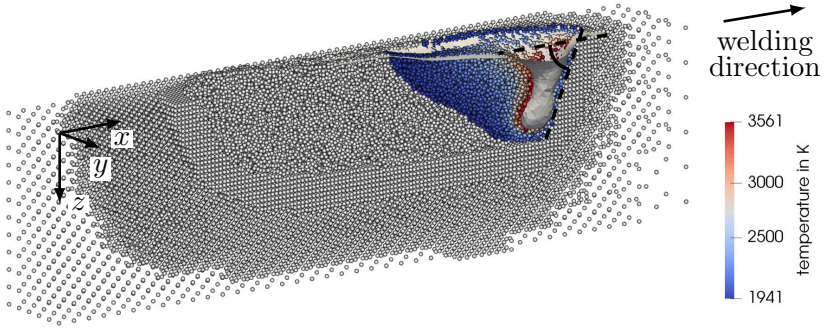

Figure 9: Capillary geometry and temperature distribution in the cross section of the melt pool during deep penetration laser beam welding of titanium at $t = 5\,\mathrm{ms}$.

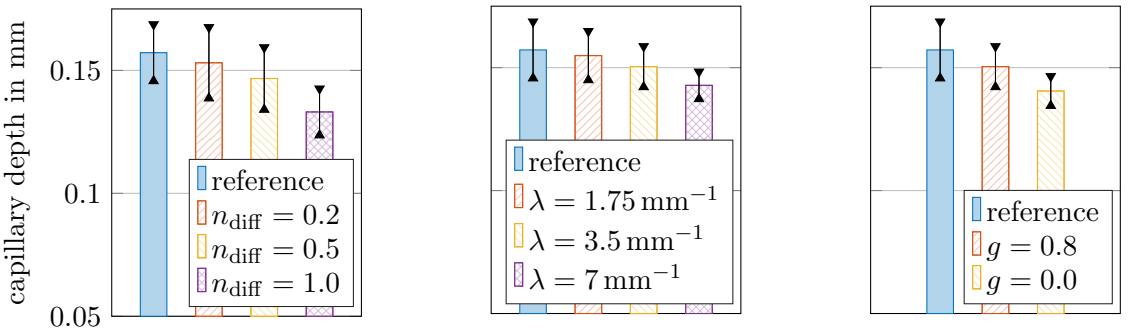

(a) only surface scattering

(b) only volume scattering, $g = 0.8$

(c) only volume scattering, $\lambda = 3.5\,\mathrm{mm}^{-1}$

Figure 10: Mean value and standard deviation (error bars) of the capillary depth in the quasi-steady state after 2 ms for deep penetration laser beam welding of titanium.

5 CONCLUSIONS

The effect of laser beam scattering is investigated simulatively for deep penetration laser beam welding. In the simulation model, the SPH method is coupled with a ray-tracing approach. The SPH model accounts for physical effects such as phase transitions, heat conduction, temperature-dependent surface tension, and evaporation-induced recoil pressure. The ray tracer calculates the energy input of the laser beam by considering multiple reflections and scattering of the light rays in the capillary.

The scattering model distinguishes between surface and volume scattering. For surface scattering, specular reflections of the rays on an ideally smooth surface are replaced by a diffuse reflection mechanism with randomly reflected rays. For volume scattering, the rays are scattered within the capillary using the Henyey-Greenstein model.

The simulation model is able to accurately capture the transient behavior of the capillary and the fluid dynamics during deep penetration laser beam welding. Without scattering, strongly correlated fluctuations in the capillary depth and the absorbed power can be seen. These fluctuations are caused by melt bridges that divide the capillary. With surface and volume scattering, a decrease in total absorbed power is observed. Due to the diffuse reflection mechanism of the surface scattering model, the absorbed laser power is large at locations where the laser beam is first reflected. In the simulation with aluminum, the first reflections are observed mainly at the capillary tip leading to a slight increase in the mean depth, while with titanium the mean depth is decreased because the first reflections are mainly at the capillary front. Volume scattering leads to a better distribution of absorbed power in the capillary. The lower recoil pressure at the capillary tip prevents the formation of melt bridges and results in a significant increase in capillary stability in the simulation of deep penetration laser beam welding of aluminum.

In this work, the influence of laser beam scattering with only an estimated choice of the scattering parameters is investigated. By measuring the physical scattering parameters, the actual effect can be further studied. In addition, a direct manipulation of the distribution of absorbed power can be examined to achieve higher capillary stability with less process instabilities, e.g., by beam shaping or adding powder to the process. Finally, the vapor phase and condensation need to be included in future research to consider their effect on the laser beam welding process.

ACKNOWLEDGMENT

The research leading to the presented results was funded by the Deutsche Forschungsgemeinschaft (DFG, German Research Foundation) in project 266218804. This support is highly appreciated.

REFERENCES

[1] Dal, M.; Fabbro, R.: An Overview of the State of Art in Laser Welding Simulation. Optics & Laser Technology, Vol. 78, pp. 2–14, 2016.

[2] Sollich, D.; Reinheimer, E.N.; Wagner, J.; Berger, P.; Eberhard, P.: An Improved Recoil Pressure Boundary Condition for the Simulation of Deep Penetration Laser Beam Welding Using the SPH Method. European Journal of Mechanics - B/Fluids (accepted for publication), 2022.

[3] Shah, D.; Volkov, A.N.: Simulations of Deep Drilling of Metals by Continuous Wave Lasers Using Combined Smoothed Particle Hydrodynamics and Ray-Tracing Methods. Applied Physics A: Materials Science & Processing, Vol. 126, No. 2, pp. 82.1–82.12, 2020.

[4] Russell, M.; Souto-Iglesias, A.; Zohdi, T.: Numerical Simulation of Laser Fusion Additive Manufacturing Processes Using the SPH Method. Computer Methods in Applied Mechanics and Engineering, Vol. 341, pp. 163–187, 2018.

[5] Fürstenau, J.P.; Wessels, H.; Weißenfels, C.; Wriggers, P.: Generating Virtual Process Maps of SLM Using Powder-scale SPH Simulations. Computational Particle Mechanics, Vol. 7, No. 4, pp. 655–677, 2020.

[6] Meier, C.; Fuchs, S.L.; Hart, A.J.; Wall, W.A.: A Novel Smoothed Particle Hydrodynamics Formulation for Thermo-Capillary Phase Change Problems with Focus on Metal Additive Manufacturing Melt Pool Modeling. Computer Methods in Applied Mechanics and Engineering, Vol. 381, p. 113812, 2021.

[7] Henyey, L.G.; Greenstein, J.L.: Diffuse Radiation in the Galaxy. The Astrophysical Journal, Vol. 93, pp. 70–83, 1941.

[8] Mie, G.: Beiträge zur Optik trüber Medien, speziell kolloidaler Metallösungen (in German). Annalen der Physik, Vol. 330, No. 3, pp. 377–445, 1908.

[9] Han, S.W.; Cho, W.I.; Zhang, L.J.; Na, S.J.: A Study on Laser Keyhole Welding in Vacuum by Computational Fluid Dynamics Simulations with Plume Effect Models. Journal of Laser Applications, Vol. 33, No. 1, pp. 012042–1 to 012042–14, 2021.

[10] Monaghan, J.J.: Smoothed Particle Hydrodynamics and Its Diverse Applications. Annual Review of Fluid Mechanics, Vol. 44, pp. 323–346, 2012.

[11] Qin, Y.; Michalowski, A.; Weber, R.; Yang, S.; Graf, T.; Ni, X.: Comparison between Ray-Tracing and Physical Optics for the Computation of Light Absorption in Capillaries – the Influence of Diffraction and Interference. Optics Express, Vol. 24, pp. 26606–26617, 2012.

[12] Hügel, H.; Graf, T.: Laser in der Fertigung - Grundlagen der Strahlquellen, Systeme, Fertigungsverfahren. Wiesbaden: Springer Vieweg, 2014.

[13] Bernardini, F.; Mittleman, J.; Rushmeier, H.; Silva, C.; Taubin, G.: The Ball-Pivoting Algorithm for Surface Reconstruction. IEEE Transactions on Visualization and Computer Graphics, Vol. 5, No. 4, pp. 349–359, 1999.

[14] Hagenlocher, C.; Lind, J.; Wagner, J.; Hummel, M.; Olowinsky, A.; Weber, R.; Graf, T.: Comparison of Heat Conduction Mode and Deep Penetration Mode by Means of High-Speed Synchrotron X-Ray Videos During Laser Beam Welding. DaRUS, 2021.

[15] Wagner, J.; Hagenlocher, C.; Hummel, M.; Olowinsky, A.; Weber, R.; Graf, T.: Synchrotron X-Ray Analysis of the Influence of the Magnesium Content on the Absorptance During Full-Penetration Laser Welding of Aluminum. Metals, Vol. 11, No. 5, p. 797, 2021.

[16] Sollich, D.; Eberhard, P.: Adaptive Smoothed Particle Hydrodynamics for the Simulation of Laser Beam Welding Processes. In Proceedings of the 15th International Smoothed Particle Hydrodynamics European Research Interest Community Workshop (SPHERIC 2021), Newark, NJ, USA, pp. 158–165, 2021.

[17] Zhao, C.; Parab, N.D.; Li, X.; Fezzaa, K.; Tan, W.; Rollett, A.D.; Sun, T.: Critical Instability at Moving Keyhole Tip Generates Porosity in Laser Melting. Science, Vol. 370, No. 6520, pp. 1080–1086, 2020.